First-principles studies of Te line-ordered alloys in a MoS_2 monolayer

N.F. Andriambelaza[a,*], R.E. Mapasha[a], N. Chetty[a,b]

[a] *Department of Physics, University of Pretoria, Pretoria 0002, South Africa*
[b] *National Institute for Theoretical Physics, Johannesburg, 2000, South Africa*

Abstract

The thermodynamic stability, structural and electronic properties of Te line-ordered alloys are investigated using density functional theory (DFT) methods. Thirty four possible Te line-ordered alloy configurations are found in a 5×5 supercell of a MoS_2 monolayer. The calculated formation energies show that the Te line-ordered alloy configurations are thermodynamically stable at 0K and agree very well with the random alloys. The lowest energy configurations at each concentration correspond to the configuration where the Te atom rows are far apart from each other (avoiding clustering) within the supercell. The variation of the lattice constant at different concentrations obey Vegard's law. The Te line-ordered alloys fine tune the band gap of a MoS_2 monolayer although deviating from linearity behavior. Our results suggest that the Te line-ordered alloys can be an effective way to modulate the band gap of a MoS_2 monolayer for nanoelectronic, optoelectronic and nanophotonic applications.

Keywords: Two dimensional materials, molybdenum disulfide, band gap.

*Corresponding author
Email address: arinala.f@gmail.com (N.F. Andriambelaza)

1. Introduction

In the past decade, two dimensional (2D) materials have gained a lot of attention in various research fields due to their potential applications in electronic, optoelectronic and photonic devices. Graphene, a single sheet of graphite, was the first 2D layered material to be synthesized successfully [1]. Although it has exotic properties such as high electron mobility, high tensile strength and high mechanical flexibility [2, 3], its major shortcoming is the absence of a band gap [4]. Recently, the novel 2D materials known as transition metal dichalcogenides (TMD) such as molybdenum disulfide (MoS_2), molybdenum diselenide ($MoSe_2$) and molybdenum ditelluride ($MoTe_2$) are becoming attractive materials for nanotechnology applications (nanoelectronic, optoelectronic and nanophotonic applications) due to their sizable band gaps as well as high charge carrier mobility [5, 6].

Similar to graphene, MoS_2 monolayer has been synthesized using mechanical exfoliation [7, 8] and chemical vapor deposition (CVD) methods [9]. The MoS_2 monolayer is a semiconductor with a direct band gap of 1.8 eV (experimentally) [10] and 1.67 eV (theoretically) [6]. This issue of band gap is of great importance in the electronic applications of a MoS_2 monolayer. Moreover, in order to optimize the application of this material, engineering of the band gap is a critical idea to investigate.

Previous studies on MoS_2 monolayer reported that alloying at the Mo and S sites can fine tune the band gap of this material [10, 11]. Xu *et al.* [10] studied the effects of tungsten (W) and selenium (Se) alloys in the MoS_2 monolayer using CVD methods. They found that W alloys fine tune the band

gap of a MoS_2 monolayer from 1.8 eV to 1.97 eV, whereas Se alloys tune from 1.8 eV to 1.55 eV. They reported that band gap engineering is important to improve the nanoscale photoelectric devices such as the sensitivity and response rate. Kuc *et al.* [11] have performed the density functional theory (DFT) calculations to study the stability and electronic properties of the $MoS_{(1-x)}Se_x$ alloys. In agreement with the experiments [10], they found that these alloys are thermodynamically stable and successfully fine tune the band gap of the MoS_2 monolayer.

Note that the challenge in the theoretical study of alloying is the atomic arrangement. Depending on the position of the dopants, we can obtain different alloy configurations such as cluster, line or just random configurations. Combining all of them together brings a huge number of configurations at each concentration. Computing the physical properties of all these configurations is impracticable using first-principles methods. Most of the previous studies on alloying [11, 12] considered only random alloys. To the best of our knowledge, a systematic study of the line-ordered alloys configurations at different concentrations has not yet explored.

In this paper, we perform first-principles calculations to study the thermodynamic stability, structural and electronic properties of the Te line-ordered alloys in a MoS_2 monolayer. Only the S sites are substituted by the Te atoms since both are chalcogen atoms. We show that the incorporation of the Te atoms significantly affects the thermodynamic stability, the lattice constant and the electronic structure of the MoS_2 monolayer.

2. Computational details

First-principles calculations using the DFT methods as implemented in the Vienna *ab-initio* simulation package (VASP) [13] are performed to study the geometric structure, thermodynamic stability and electronic properties of the Te line-ordered alloys in a MoS_2 monolayer. The calculations are carried out in a 5×5 supercell of a MoS_2 monolayer. The generalized gradient approximation (GGA) parameterized by Perdew, Burke, and Ernzerhof (PBE) [14] is employed for the exchange-correlation potential. In DFT calculation, the standard GGA exchange-correlation is known to give an underestimated value of the pristine MoS_2 band gap [15]. The Heyd, Scuseria, and Ernzerhof exchange-correlation functional (HSE06) [16] has been proven to accurately predict the MoS_2 band gap values close to experimental values [17]. In this study, we compare the band gap value obtained using GGA exchange-correlation with the band gap obtained using HSE06 for the Te line-ordered alloys. In all the calculations, the projector augmented wave (PAW) method [18] is used for the pseudopotential generation. After convergence tests, a plane wave cutoff energy of 300 eV is considered. A k-grid of $2 \times 2 \times 1$ is used to sample the Brillouin zone. Both the lattice constants and atomic positions are fully relaxed. The relaxation convergence of energy is taken as 10^{-5} eV and the Hellmann-Feynman force between each atom set to less than 0.02 eV/Å. A vacuum spacing of 15 Å is used to isolate the single layer of MoS_2 and to suppress the spurious interlayer interaction along the z-axis.

The relative stabilities of the various possible Te line-ordered alloy con-

figurations are evaluated by calculating the formation energies given by:

$$E_{form} = E_{MoTe_xS_{1-x}} - (1-x)E_{MoS_2} - xE_{MoTe_2} \ , \tag{1}$$

where $E_{MoTe_xS_{1-x}}$, E_{MoS_2} and E_{MoTe_2} are the total energies of the mixed compound, the pristine MoS_2 and $MoTe_2$ monolayers, respectively. The x parameter is the concentration of Te atoms introduced in the MoS_2 monolayer [19].

3. Results and discussion

3.1. Structural aspects

In this study, the hexagonal structure of a MoS_2 monolayer is considered, since it has been reported that it is the most stable structure amongst different polytypes of MoS_2 monolayers [6]. Top view of this structure is shown in Fig. 1. It can be seen at a glance from Fig. 1 that the hexagonal MoS_2 monolayer is composed of three layers, one layer of the molybdenum (Mo) atoms sandwiched between two layers of the sulfur (S) atoms.

As mentioned above, we are interested in the study of the Te line-ordered alloys in a MoS_2 monolayer. To obtain the various unique Te line-ordered alloy configurations, we selectively consider the S atom sites along the zigzag of the MoS_2 monolayer. When applying this idea, the periodic boundary condition is always obeyed. The line formed by the S atoms along the zigzag is denoted by letter L shown in Fig. 1. L_1, L_2, L_3, L_4 and L_5 represent respectively the first, second, third, forth and fifth line of the S atoms along the zigzag. The letter u and b represent the upper and bottom layers of the S atoms respectively. There are ten possible rows of S atoms in a 5×5

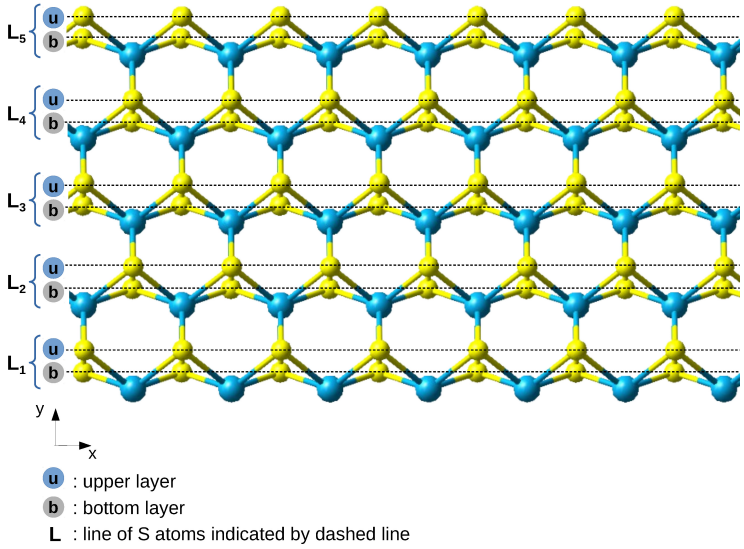

Figure 1: An hexagonal structure of a MoS_2 monolayer. The blue spheres indicate the Mo atoms and the light yellow spheres indicate the S atoms. u stand for upper layer and b for the bottom layer of the S atoms. L_1, L_2, L_3, L_4 and L_5 indicate respectively the first, second, third, forth and fifth line of S atoms along the zigzag in the 5 $\times$ 5 supercell of a MoS_2 monolayer.

supercell, five in the upper layer and the other five in the bottom layer (see Fig. 1).

Depending on the position of the Te atoms, various unique line-ordered alloys configurations can be possible at different concentrations of the Te atoms. In this work, five concentrations are chosen as $x = 0.1$ (10%), $x = 0.3$ (30%), $x = 0.5$ (50%), $x = 0.7$ (70%)and $x = 0.9$ (90%). For each concentration, different unique Te line-ordered alloy configurations are identified. We found thirty four possible unique Te line-ordered configurations: one configuration for 10%, eight configurations for 30%, sixteen configurations for 50%, eight configurations for 70% and one configuration for 90% as summarized

in Table. 1.

To better understand how to identify the Te line-ordered alloys, consider for instance the configuration L_{1u} at $x = 0.1$ (see Table. 1). It is constituted by the Te atoms substituting the upper (u) row of S atoms in line 1 (L_{1u}), denoted as $C_{1(0.1)}$. The configuration L_{1b} should be a possible configuration but due to the symmetry translation, it is the same as L_{1u}. To avoid double counting, the configuration $C_{1(0.1)}$ is the only possible configuration at $x = 0.1$. Therefore, double counting has been carefully avoided even at high concentration. For $C_{1(0.3)}$ given as $L_{1ub}L_{2u}$, the Te atoms occupy three rows

Table 1: Various Te line-ordered configurations at different concentrations.

	Concentration x				
Conf.	$x = 0.1$	$x = 0.3$	$x = 0.5$	$x = 0.7$	$x = 0.9$
C_1	L_{1u}	$L_{1ub}L_{2u}$	$L_{1ub}L_{2u}L_{3u}L_{4u}$	$L_{2ub}L_{3u}L_{4ub}L_{5ub}$	$L_{1b}L_{2ub}L_{3ub}L_{4ub}L_{5ub}$
C_2	-	$L_{1ub}L_{3b}$	$L_{1ub}L_{2ub}L_{3u}$	$L_{1u}L_{2u}L_{3u}L_{4ub}L_{5ub}$	-
C_3	-	$L_{1u}L_{2u}L_{3u}$	$L_{1ub}L_{2u}L_{3ub}$	$L_{1b}L_{2u}L_{3u}L_{4ub}L_{5ub}$	-
C_4	-	$L_{1u}L_{2u}L_{3b}$	$L_{1u}L_{2u}L_{3u}L_{4u}L_{5u}$	$L_{2u}L_{3ub}L_{4ub}L_{5ub}$	-
C_5	-	$L_{1u}L_{2u}L_{4u}$	$L_{1u}L_{2u}L_{3u}L_{4u}L_{5b}$	$L_{1ub}L_{2u}L_{3u}L_{4ub}L_{5u}$	-
C_6	-	$L_{1u}L_{2u}L_{4b}$	$L_{1u}L_{2u}L_{3u}L_{4b}L_{5b}$	$L_{1b}L_{2b}L_{3ub}L_{4u}L_{5ub}$	-
C_7	-	$L_{1u}L_{2b}L_{3u}$	$L_{1b}L_{2u}L_{3b}L_{4u}L_{5b}$	$L_{1b}L_{2u}L_{3b}L_{4ub}L_{5ub}$	-
C_8	-	$L_{1u}L_{2b}L_{4u}$	$L_{1ub}L_{2ub}L_{4u}$	$L_{1ub}L_{2b}L_{3ub}L_{4u}L_{5b}$	-
C_9	-	-	$L_{1ub}L_{2u}L_{3u}L_{4b}$	-	-
C_{10}	-	-	$L_{1ub}L_{2u}L_{3u}L_{5u}$	-	-
C_{11}	-	-	$L_{1ub}L_{2u}L_{3u}L_{5b}$	-	-
C_{12}	-	-	$L_{1ub}L_{2b}L_{3u}L_{5b}$	-	-
C_{13}	-	-	$L_{1ub}L_{2u}L_{3b}L_{5b}$	-	-
C_{14}	-	-	$L_{1ub}L_{2b}L_{3u}L_{4u}$	-	-
C_{15}	-	-	$L_{1ub}L_{2u}L_{3b}L_{4u}$	-	-
C_{16}	-	-	$L_{1ub}L_{2b}L_{4ub}$	-	-

of the S atoms. The upper (u) and bottom (b) rows of S atoms in L_1, and the upper (u) row of S atoms in L_2 are occupied. Following the same procedure, different unique configurations are possible at $x = 0.3$ to $x = 0.9$ as summarized in Table. 1. The atomic positions as well as the lattice constants of all Te line-ordered alloys configurations are optimized in order to study their relative thermodynamic stabilities and also to identify the lowest energy configuration at each concentration.

3.2. Thermodynamic stabilities of the Te line-ordered alloys

The feasibility and stability of the Te line-ordered alloy configurations are investigated by calculating the formation energy using Eq. 1. The formation energies of each configuration in Table. 1 are summarized in Table. 2. The calculated values allow us to recognize the lowest energy configuration at each concentration.

At $x = 0.1$ only one configuration $C_{1(0.1)}$ is possible, and has the lowest formation energy as compared to those of high concentration as shown in Table. 1. For comparison purpose, we used the special quasirandom structure (SQS) algorithm [20] to identify unique random alloy configurations at 10% (x=0.1) only. Few of the selected configurations are shown in Fig. 2. These random configurations are similar to those reported in Ref. [21, 22] for Se and Te alloys. We found that the formation energy of the $C_{1(0.1)}$ although slightly higher by 0.002 eV on average, compares very well with those of random alloys. Even though the formation energies are positive, their magnitudes are very small, on the order of ∼meV. Our random alloy configurations formation energies are in good agreement with those reported by Kang *et al.* [23], who argued that these types of system can be synthesized at experimentally

achievable temperatures. Therefore, since the formation energy of the $C_{1(0.1)}$ line-ordered alloy compares very well with those of random alloys, both systems should be synthesized at the same conditions.

At 30% concentration, configuration $C_{8(0.3)}$ is the most stable structure

Table 2: Formation energies of the various Te line-ordered configurations at different concentrations. The bold values indicate the lowest energy at each concentration.

	Formation energies (meV)				
Conf.	$x = 0.1$	$x = 0.3$	$x = 0.5$	$x = 0.7$	$x = 0.9$
C_1	**7.6**	18.9	34.4	16.8	**7.5**
C_2	-	16.7	24.7	35.1	-
C_3	-	30.2	21.3	16.2	-
C_4	-	15.6	66.0	20.6	-
C_5	-	28.2	31.4	33.0	-
C_6	-	16.2	16.7	15.6	-
C_7	-	12.9	**12.8**	15.4	-
C_8	-	**12.2**	22.1	**14.1**	-
C_9	-	-	17.4	-	-
C_{10}	-	-	35.6	-	-
C_{11}	-	-	19.4	-	-
C_{12}	-	-	18.7	-	-
C_{13}	-	-	18.2	-	-
C_{14}	-	-	18.8	-	-
C_{15}	-	-	15.7	-	-
C_{16}	-	-	19.1	-	-

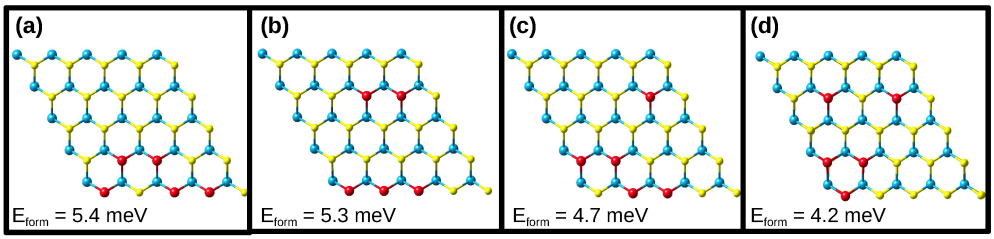

Figure 2: Selected different random alloy configurations at 10% (x= 0.1) consisting of 5Te substituting S atoms.

and configuration $C_{3(0.3)}$ is the most unstable one. The configuration $C_{8(0.3)}$ corresponds to the configuration $L_{1u}L_{2b}L_{4u}$ (see Table. 1), where the Te atoms occupy the upper (u) row of S atoms in L_1, the bottom (b) row of S atoms in L_2 and the upper (u) row of S atoms in L_4 as seen in Fig. 3b. Contrary, the highest energy configuration ($C_{3(0.3)}$) is the configuration where the rows of the Te atoms are settled next to each other and occupy the same layer as $L_{1u}L_{2u}L_{3u}$ (see Table. 1). We realized that the formation energies of the configurations depend on the separation of the Te atom rows within the supercell. In the highest energetically configuration $C_{3(0.3)}$, all the three Te rows are close to each other, each separated by 3.27 Å on the upper layer. In configuration $C_{8(0.3)}$, $L_{1u}L_{2b}L_{4u}$, the two Te rows $L_{1u}L_{2b}$ are separated by 4.46 Å, but the third row L_{4u} is relatively far 7.08 Å away within the supercell, and this is the most stable configuration. Considering the periodic boundary condition as usual, L_{4u} row is 6.34 Å away from L_{1u} in the next cell, thus this separation is still large making the structure stable. Nevertheless, due to very smaller energy difference, both configurations can be achieved experimentally under the same conditions. The same observation is found

at 50% (as seen in Fig. 3c) and at 70% (as seen in Fig. 3d). Note that the highest formation energy value is found at around 70%. This trend is in agreement with the results of Rajbanshi *et. al.* on the study of Se and Te random alloy configurations [21] and they argued that the formation of such kind of alloys is greatly composition dependent. In general, the Te alloys prefer to be at a distance far away from each other as opposed to transition metal alloys where the substituted atoms prefer to be next to each other [11].

The introduction of the Te line-ordered alloys affects the lattice constant of the MoS_2 monolayer since the atomic size of the Te atoms is larger than that of the S atoms. Fig. 4 shows the lattice constant of the lowest energy configuration at each concentration ($C_{1(0.1)}$, $C_{8(0.3)}$, $C_{7(0.5)}$, $C_{8(0.7)}$ and $C_{1(0.9)}$). We can see in Fig. 4 that the lattice constant increases linearly with the increase in concentration. The lattice constant values vary between the lattice constants of a MoS_2 monolayer (3.18 Å) and a $MoTe_2$ monolayer

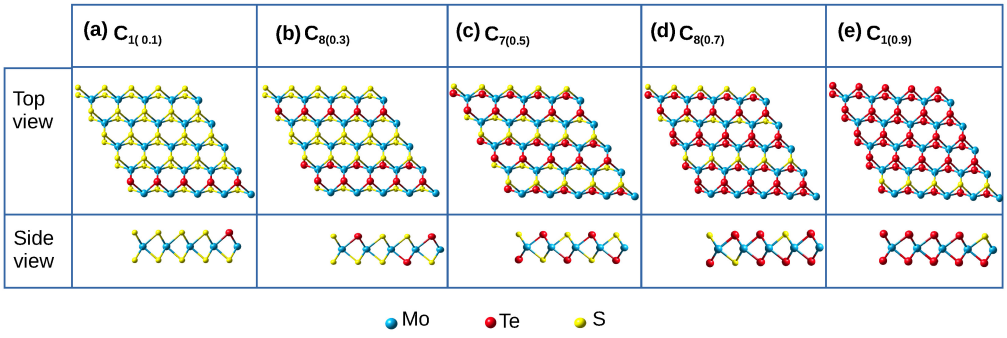

Figure 3: Top view and side view of the lowest energy configuration at (a) 10%, configuration $C_{1(0.1)}$; (b) 30%, configuration $C_{8(0.3)}$; (c) 50%, configuration $C_{7(0.5)}$; (d) 70%, configuration $C_{8(0.7)}$ and (e) 90%, configuration $C_{1(0.9)}$.

(3.54 Å). Indeed, the Te line-ordered alloys cause an outward strain in the system and the lattice constant obey Vegard's law. This behavior has already been experimentally found in the 2D TMD random alloys [24].

3.3. Electronic properties of the Te line-ordered alloys

Both 2D MoS_2 and $MoTe_2$ monolayers are semiconductor materials with the band gap values of 1.65 eV ($x = 0$ in Fig. 6) and 1.04 eV ($x = 1$ in Fig. 6), respectively. These values are in agreement with the values reported in Refs. [6, 24]. To explore the effects of the Te line-ordered alloys on the electronic properties of the MoS_2 monolayer, we calculate the total density of states (TDOS) at each concentration. Fig. 5 shows the TDOS of the lowest energy configurations at each concentration. Then, the magnitudes of the band gap at each concentration are measured and plotted in Fig. 6. The black (red) line indicates the band gap of the Te line-ordered alloys at

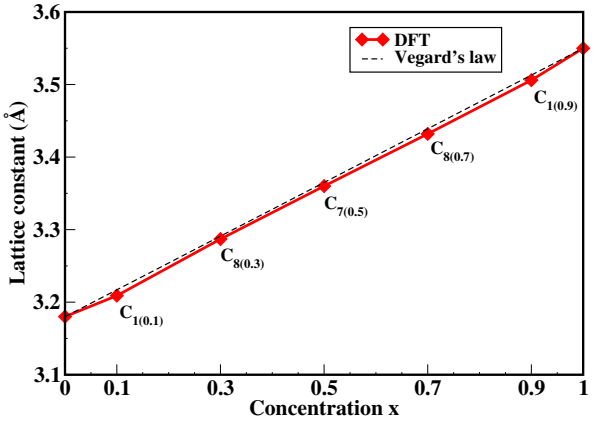

Figure 4: The lattice constants for the lowest energies configurations of the Te line-ordered alloys at different concentration (red line). The black dashed line shows the lattice constants obtained by using Vegard's law.

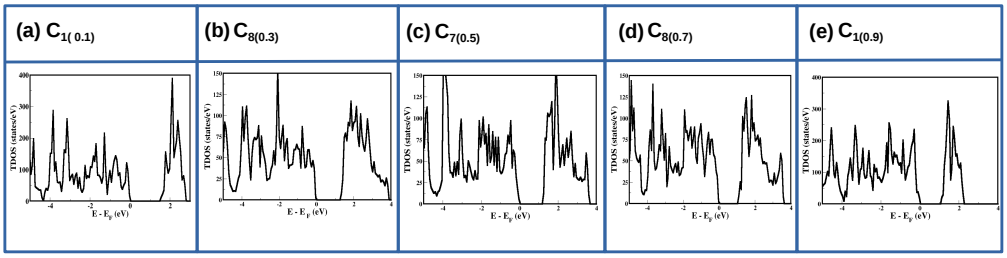

Figure 5: Total density of states (TDOS) for the lowest energy configurations at each concentration.

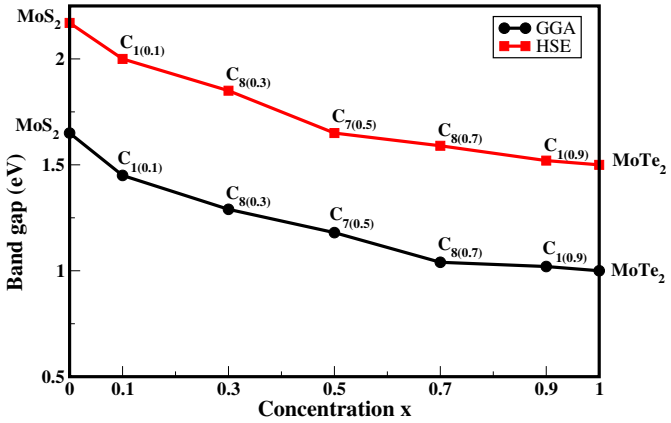

Figure 6: The calculated band gaps of the lowest energy configurations at each concentration. The black and red lines are the band gaps obtained using GGA and HSE exchange-correlation, respectively.

different concentrations using GGA (HSE) exchange-correlation functional. The values of the band gap decrease with the increase in Te concentration towards that of $MoTe_2$ monolayer (see Fig. 6). Unlike the lattice constant, the plot of the band gap deviates from the linearity behavior. The Te line-ordered alloys fine tune the band gap of the pristine MoS_2 monolayer from 1.65 eV (2.17 eV) to 1.04 eV (1.48 eV) using GGA(HSE) exchange-correlation

functional. The magnitudes of the band gaps depend on the composition of the alloys and cover the range of visible spectrum. Therefore, these materials can be used in solar related applications, for example as an absorber in a solar cell.

Fig. 6 compares the GGA and HSE band gap values. We realize that the HSE values are higher than that of GGA for the entire plots. However, the trend of the band gap plots (black line in Fig. 6 for GGA and red line for HSE) is the same. This indicates that the GGA functional can give a qualitative description of the electronic structure of various alloys in TMD materials.

4. Conclusion

In conclusion, using the density functional theory method, the lowest energy configuration at each concentration for the Te line-ordered alloys in a MoS_2 monolayer has been identified to optimize the applications of the 2D MoS_2 in the nanotechology devices. The calculated formation energies show that the Te line-ordered alloy configurations are thermodynamically stable at 0K and compete very well with the random alloys. The Te line-ordered alloys affect the lattice constant as well as the electronic properties of the MoS_2 monolayer. The lattice constant variation obeys Vegard's law and the band gap of the 2D MoS_2 is tuned between 1.65 eV and 1.04 eV. The range of band gap is related to the solar spectrum, indicating the importance of this study in nanoelectronic and nanophotonic, more especially in solar cell related devices.

Acknowledgment

The authors wish to thank the University of Pretoria for financial assistance. NRF and NIThep are greatly acknowledged.

References

[1] K. S. Novoselov, A. K. Geim, S. V. Morozov, D. Jiang, Y. Zhang, S. V. Dubonos, I. V. Grigorieva, A. A. Firsov, science 306 (5696) (2004) 666–669.

[2] J.-H. Chen, C. Jang, S. Xiao, M. Ishigami, M. S. Fuhrer, Nat. Nanotech. 3 (4) (2008) 206–209.

[3] C. Lee, X. Wei, J. W. Kysar, J. Hone, science 321 (5887) (2008) 385–388.

[4] A. C. Neto, F. Guinea, N. M. Peres, K. S. Novoselov, A. K. Geim, Rev. Mod. Phys. 81 (1) (2009) 109.

[5] X.-B. Li, P. Guo, Y.-N. Zhang, R.-F. Peng, H. Zhang, L.-M. Liu, J. Mater. Chem. C 3 (24) (2015) 6284–6290.

[6] F. A. Rasmussen, K. S. Thygesen, J. Mater. Chem. C 119 (23) (2015) 13169–13183.

[7] J. Wu, H. Li, Z. Yin, H. Li, J. Liu, X. Cao, Q. Zhang, H. Zhang, Small 9 (19) (2013) 3314–3319.

[8] I. Song, C. Park, H. C. Choi, RSC Advances 5 (10) (2015) 7495–7514.

[9] Y.-H. Lee, X.-Q. Zhang, W. Zhang, M.-T. Chang, C.-T. Lin, K.-D. Chang, Y.-C. Yu, J. T.-W. Wang, C.-S. Chang, L.-J. Li, et al., Adv. Mater. 24 (17) (2012) 2320–2325.

[10] W. Zhang, X. Li, T. Jiang, J. Song, Y. Lin, L. Zhu, X. Xu, Nanoscale 7 (32) (2015) 13554–13560.

[11] A. Kuc, T. Heine, Electronics 5 (1) (2015) 1.

[12] H.-P. Komsa, A. V. Krasheninnikov, J. Phys. Chem. Lett. 3 (23) (2012) 3652–3656.

[13] G. Kresse, J. Furthmüller, Comput. Mater. Sci. 6 (1) (1996) 15–50.

[14] J. P. Perdew, K. Burke, M. Ernzerhof, Phys. Rev. Lett. 77 (18) (1996) 3865.

[15] N. F. Andriambelaza, E. Mapasha, N. Chetty, J. Phys. Condens. Matter.[link].
URL http://iopscience.iop.org/10.1088/1361-648X/aa7a22

[16] J. Heyd, G. E. Scuseria, M. Ernzerhof, J. Chem. Phys. 118 (18) (2003) 8207–8215.

[17] M. Faraji, M. Sabzali, S. Yousefzadeh, N. Sarikhani, A. Ziashahabi, M. Zirak, A. Moshfegh, RSC Advances 5 (36) (2015) 28460–28466.

[18] P. E. Blöchl, Phys. Rev. B 50 (24) (1994) 17953.

[19] T. L. Tan, M.-F. Ng, G. Eda, J. Phys. Chem. C 120 (5) (2016) 2501–2508.

[20] A. Zunger, S.-H. Wei, L. Ferreira, J. E. Bernard, Phys. Rev. Lett. 65 (3) (1990) 353.

[21] B. Rajbanshi, S. Sarkar, P. Sarkar, Phys. Chem. Chem. Phys. 17 (39) (2015) 26166–26174.

[22] Q. Feng, Y. Zhu, J. Hong, M. Zhang, W. Duan, N. Mao, J. Wu, H. Xu, F. Dong, F. Lin, et al., Advanced Materials 26 (17) (2014) 2648–2653.

[23] J. Kang, S. Tongay, J. Li, J. Wu, J. Appl. Phys. 113 (14) (2013) 143703.

[24] S. Srivastava, D. Palit, Solid State Ion. 176 (5) (2005) 513–521.